Cryogenic nanoscale etching of silicon nitride selectively to silicon by alternating SiF 4 /O 2 and Ar plasmas

Gaelle Antoun, Thomas Tillocher, Aurélie Girard, Philippe Lefaucheux, J. Faguet, H. Kim, D. Zhang, M. Wang, K. Maekawa, Christophe Cardinaud, et al.

Cryogenic nanoscale etching of silicon nitride selectively to silicon by alternating SiF_4/O_2 and Ar plasmas

G. Antoun[1*], T. Tillocher[1], A. Girard[2], P. Lefaucheux[1], J. Faguet[3], H. Kim[4], D. Zhang[4], M. Wang[4], K. Maekawa[4], C. Cardinaud[2], R. Dussart[1*]

[1]GREMI, Orléans University-CNRS, 14 Rue d'Issoudun BP 6744, 45067 Orléans, France

[2]IMN, Institut des Matériaux Jean Rouxel, Université de Nantes, CNRS, BP32229, 44322 Nantes Cedex 3, France

[3]Tokyo Electron America, Inc., 2400 Grove Blvd., Austin, Texas 78741, USA

[4]TEL Technology Center, America, LLC, NanoFab 300 South 255 Fuller Rd., Suite 214, Albany, NY, USA

* remi.dussart@univ-orleans.fr

Abstract

This article first presents quasi *in situ* XPS measurements on Si_3N_4 and a-Si samples after exposure to a SiF_4 / O_2 plasma at different cryogenic temperatures. A different behavior is observed between the two materials at -65°C, which has led to the development of a time-multiplexed process for nanoscale etching. This study clearly shows the possibility to switch from a deposition regime to an etching regime by decreasing the temperature. The threshold temperature between these regimes being different for both materials, it was possible to perform selective etching of Si_3N_4 over a-Si by wisely choosing the temperature.

I. Introduction

Cryogenic Atomic Layer Etching (Cryo-ALE) has been first proposed to etch SiO_2 thin layers while limiting reactor wall contamination. It consists of an alternating process: the substrate is cooled below -90°C in order to enable the physisorption of a gas during the modification step. In reference [1], we have reported on a Cryo-ALE process using C_4F_8 as a proof of principle of this technique. According to Antoine's curve [2], the pressure and temperature necessary conditions for the condensation of C_4F_8 can be reached by a cryogenic etching tool. However, even if a self-limiting etching regime was obtained for SiO_2, the selectivity over Si and Si_3N_4 remained quite low.

In reference[3 4], the authors investigated ALE of Si_3N_4 by physisorbing HFC gas during the modification step. In this study, the substrate was kept at 80°C and the pressure was increased. They demonstrated the feasibility of the process and the etching enhancement by adding hydrogen during the modification step. But, the selectivity towards other materials has not been discussed in this paper.

The selectivity for Si_3N_4 etching over Si and SiO_2 has been widely studied using fluorine based gases and more specifically hydrofluorocarbon gases for continuous etching [5–15], but also for atomic layer etching processes [16–31]. It was shown that hydrogen plays a key role in the etching of Si_3N_4 and the selectivity. For example, when a hydrogen atom released in the plasma reaches the surface, it reacts with the nitrogen present in the layer creating volatile NH_3 products. Thus it creates a Si rich layer with dangling bonds allowing fluorine atoms to react with silicon [32,33]. The etching of Si_3N_4 can also be obtained indirectly by forming ammonium salt $(NH_4)_2SiF_6$, which can be removed by annealing as reported in [20,31].

Recently, Hsiao *et al.* demonstrated the effect of temperature on the etch rate of Si_3N_4 layers deposited by PECVD and etched by CF_4 / H_2 plasma. They showed that the etch rate of films rich in Si-H bonds can be increased by decreasing the temperature to -20°C, while the etch rate decreases for films rich in N-H bonds [32].

In this article, the etching of Si_3N_4 films using SiF_4 / O_2 plasma is investigated for temperatures below -40°C. The silicon oxyfluoride (SiO_xF_y) layer formed in such low temperature conditions, usually known as the passivation layer in Si cryoetching [34–40], is used to etch Si_3N_4 while preventing a-Si etching.

Indeed, in cryogenic standard deep etching, SiF_x species formed during the etching react with oxygen to create a SiO_xF_y layer. The low temperature enables to enhance the surface residence time of SiF_x species on the surface, which favors their reaction with oxygen radicals from the plasma [34,41].

It was shown in reference [34] that SiF_x species (with x < 4) were involved in the formation of the passivation layer, and that SiF_4 molecules were not physisorbing in the pressure and temperature conditions used for the experiment. Recently, quasi *in situ* XPS experiments carried out on a-Si showed that exposing the surface to a SiF_4 / O_2 plasma at temperatures higher than about -65°C leads to the fluorination of the native oxide layer and the formation of chemisorbed stable layer [42]. If the temperature is further decreased, down to -100°C, the physisorption of fluorinated species is enhanced. It is thus proposed in this article to take advantage of these properties obtained at low temperature to create a selective nanoscale etch process of Si_3N_4.

II. Experimental methods

The experiments were conducted on a-Si and Si_3N_4 layers deposited on Si substrates. The 50 nm thick a-Si layer was first grown on 100 nm thick SiO_2. The Si_3N_4 layer is about 240 nm thick, directly deposited on the Si substrate by LPCVD.

20 x 20 mm² coupons were glued on a 6" SiO_2 carrier wafer using a special glue with high thermal conductivity. Two different Inductively Coupled Plasma reactors (ICP) were used: one for process tests using in-situ ellipsometry at GREMI-Orléans and the other one dedicated to XPS quasi-in situ experiments at IMN-Nantes.

A sketch of the first one can be found in reference [43]. In this reactor, the temperature is measured by a PT100 sensor, which is mounted in the chuck. An *in situ* UVISEL Horiba Jobin Yvon spectroscopic ellipsometer (SE) is coupled to this reactor in order to monitor the thickness evolution in mono acquisition and kinetic modes during processes. To model and fit the a-Si and the Si_3N_4 materials, new amorphous dispersion formulas are used. In addition, when the deposited layer is thick enough (more than about 3 nm), a classical dispersion formula is added to the model. Fig. 1 (a) and (b) show an example of the ellipsometric parameters Is and Ic measured and fitted by SE after deposition of a SiO_xF_y layer on a-Si and Si_3N_4 respectively. The created model fits the measurements with an error value χ^2 typically lower than 5. At 1.96

eV, the refractive indexes for the SiO_xF_y layer obtained in our experimental conditions (T = -40°C; SiF_4 / O_2: 25%; Source power: 1500 W; Pressure: 1.2 Pa; Process duration: 30 s) are 1.59 and 1.45 when deposited on a-Si and Si_3N_4 respectively.

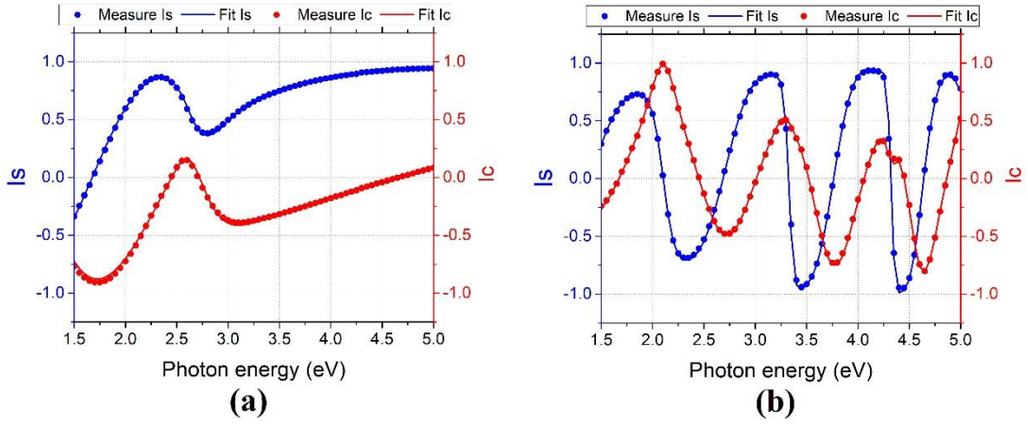

Fig. 1. Ellipsometric parameters *Is* and *Ic* measured and fitted as a function of the photon energy for a SiO_xF_y layer deposited at -40°C on (a) a-Si, (b) Si_3N_4 (Experimental conditions: SiF_4 / O_2: 25%, Source: 1500 W, 1.2 Pa, 30 s)

The second ICP tool used is the OPTIMIST platform (Opening of a Technical Platform for the Investigation of the Mechanisms of Interaction between plasma and Surface on a large Temperature range) and is presented in details in Fig. 2. It is a homemade ICP reactor operating at 13.56 MHz coupled to an X-ray Photoelectron Spectroscope (XPS) equipment, which allows quasi *in situ* analysis of the treated samples. 10 x 10 mm² coupons are loaded on a moving sample rod and cooled to a low temperature. In this experimental setup, a Ni/NiCr thermocouple is welded onto the backside of the sample holder to measure the temperature. The sample holder is controlled in temperature by liquid nitrogen down to -180°C and the rod can be moved from the reactor chamber to the XPS chamber while keeping the sample at the desired temperature and at low pressure ($<10^{-5}$ Pa).

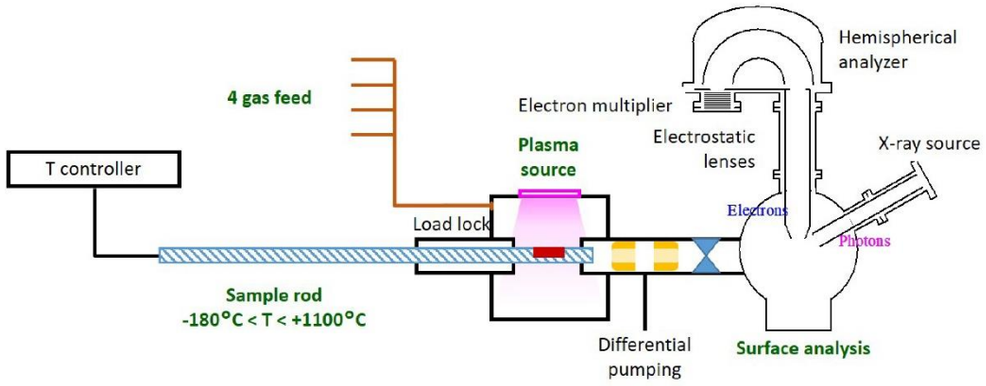

Fig. 2. Sketch of the OPTIMIST Platform

No pre-treatment was applied to the samples. Each experiment was performed separately on each material and an O_2 / Ar plasma cleaning process was performed before each experiment. XPS analysis was carried out with an Al Kα monochromatised x-ray source (SPECS XR 50M and Focus 500) operated at 400 W. The x-spot at the surface is 2 x 2 mm^2 and is centered at the middle of the sample. Quantification results presented below are thus averaged over the probed area and naturally averaged over the probed depth.The analyser (SPECS Phoibos 150HR) operates in fixed transmission and medium area mode. Survey scans were acquired at 30 eV pass energy (PE) with 0.5 eV steps, and high resolution narrow scans at 14 eV PE with 0.05 eV steps. The software used for the XPS data analysis is Casa XPS [44].

III. Results

III.1 Characterization of the deposited layer as a function of temperature

In order to study the effect of temperature, the samples were exposed to a SiF_4 / O_2 plasma for 30 s in the first ICP reactor. 10 sccm of SiF_4 and 30 sccm of O_2 were injected in order to have 25% of SiF_4 in the mixture. The pressure was set at 1.2 Pa, the plasma source power was 1500 W and no bias was applied. The tested temperatures were -40°C, -65°C and -100°C.

Fig. 3 shows the results obtained for the two materials: a-Si and Si_3N_4. At -40°C, a SiO_xF_y layer of about 13 to 14 nm thickness was deposited on both materials. When the temperature was decreased to -65°C, the deposited amount of SiO_xF_y slightly decreased on a-Si, and dropped to 4.7 nm on Si_3N_4. At -100°C, a significant change is observed on both materials. Almost no deposition was obtained on a-Si, whereas a 3.7 nm thick layer of Si_3N_4 was etched on the Si_3N_4 coupon.

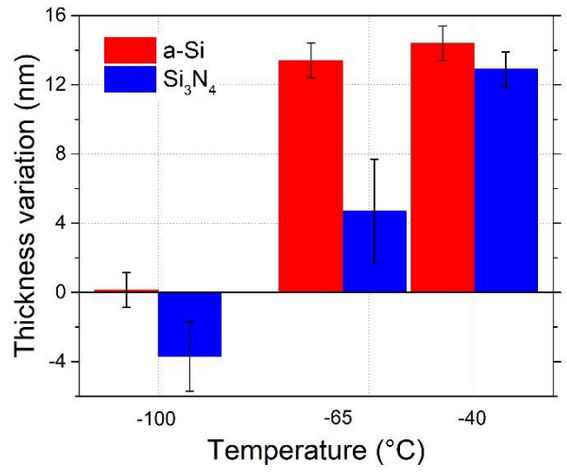

Fig. 3. Thickness variation of a-Si and Si_3N_4 at different temperatures, after SiF_4 / O_2 plasma

(Experimental conditions: SiF_4 / O_2: 25%, Source: 1500 W, 1.2 Pa, 30 s)

In order to understand this difference of behavior between both materials when decreasing the temperature, quasi *in situ* XPS measurements were performed using the second ICP reactor (OPTIMIST). The used plasma parameters were adapted to the facility (smaller volume): 6 sccm of SiF_4 and 20 sccm of O_2 were injected into the reactor to maintain the ratio of 25% of SiF_4 in the mixture. The plasma source power was decreased to 200 W and the pressure increased to 3.0 Pa. The process duration was 30 s as in the first ICP reactor.

Fig. 4 presents the a-Si and Si_3N_4 surface composition just after exposure to SiF_4 / O_2 plasma and after warming the samples up to room temperature. These quantification results are

averaged over the probed depth, except at -100°C. In this case, as detailed below, the quantification results do not reflect the real structure of the analyzed depth because a physisorbed layer is present at the sample surface. The results obtained on a-Si are presented in detail in reference [42]. It is mainly shown that at -40°C and -65°C, F-rich species from the SiF_4 / O_2 plasma chemisorb at the surface, fluorinating the native silicon oxide layer (Fig. 4 (a)). At -100°C, the physisorption of fluorinated species is drastically enhanced: the fluorine content reaches 52%, which indicates that the surface is mainly covered by fluorinated physisorbed species.

The reference atomic concentration shown for Si_3N_4 in Fig. 4 (b) corresponds to the reference sample used for the deposition at -40°C. Note that this concentration and the amounts of N and O vary a little for the three Si_3N_4 used. This is partially due to the C contamination amount that also varies on the surface, and thus affects the calculation of the surface concentrations. But this amount difference does not affect the interpretation of the results.

After exposure at -40°C and -100°C, the composition evolution of a-Si and Si_3N_4, with respect to the reference, is quite similar. At -40°C, the carbon present initially at the surface as superficial contamination is almost no longer detected. Resulting from the plasma exposure, 15 to 17% of fluorine content is evaluated. This proportion remains quite constant even after heating the samples.

At -100°C, as obtained for a-Si, the Si_3N_4 surface is mainly covered by chemisorbed and physisorbed species with a fluorine content as high as of 52%. Contribution of the substrate, a-Si or Si_3N_4, is no longer observable. After heating, a significant part of the physisorbed layer desorbs, and the Si signal (and N for Si_3N_4) from the substrate is detected again.

The surface compositions of the samples after the deposition at -40°C or -100°C and after heating to 20°C are also quite similar. This shows that the remaining layer surface is composed of chemisorbed species and is stable in the range of the studied temperatures (-100°C to 20°C).

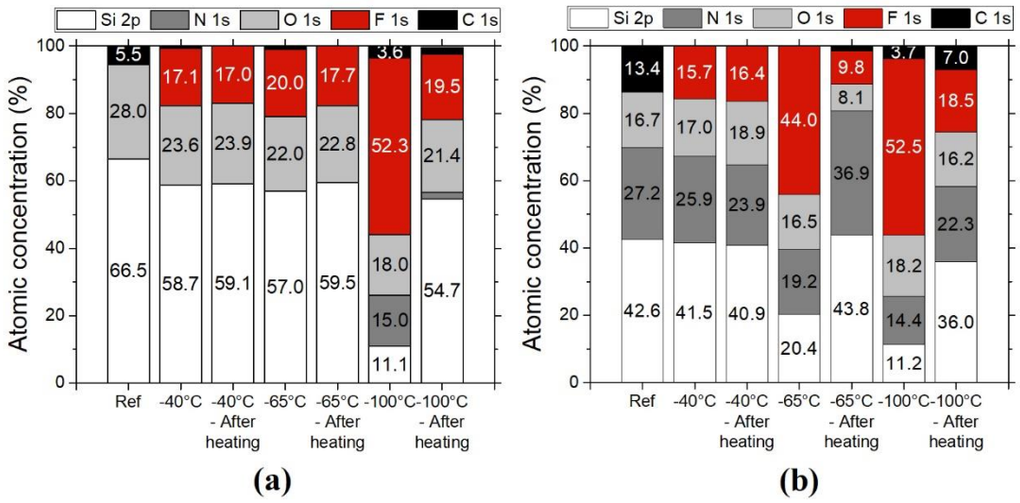

Fig. 4. XPS average quantification of the surface composition after SiF_4 / O_2 plasma and after warming the sample back to 20°C, (a) on a-Si and (b) on Si_3N_4 (Experimental conditions: SiF_4 / O_2 plasma: 25%, 30 s, 3 Pa, 200 W)

In agreement with the results shown in Fig. 3, the main difference between the two materials is observed at -65°C as expected.

At this temperature, the a-Si material has a similar behavior as at -40°C, with only chemisorbed fluorine based species on the native oxide layer. But, on Si_3N_4 material, the fluorine content after deposition is drastically enhanced and reaches a value of 44% of the surface composition. After heating, as at -100°C, a significant part of it desorbs, as the fluorine content drops to 9.8% only at the surface. Note that the high percentage of N detected at this temperature (36.9 % instead of 20-25%) is the same as the initial composition of the raw surface of the sample used for this test at -65°C.

The spectra for both a-Si and Si_3N_4 are plotted in Fig. 5 after exposure to SiF_4 / O_2 plasma at -65°C in order to better understand the involved surface mechanisms for the two materials at this temperature. The XPS measurements were performed while the sample was maintained at -65°C. In the survey scans presented in Fig. 5 (a) the main difference between the two materials is the intensity of the F 1s spectrum observed on Si_3N_4 which is much higher than the one

obtained on a-Si at the same temperature. A narrow scan of the F 1s core level is presented in Fig. 5 (b). For a-Si, one main peak is detected and can be decomposed into two peaks corresponding to F-Si(O) bonds located at 687.3 eV and 685.48 eV [45,46]. For Si_3N_4, the main F 1s peak can also be decomposed into two peaks located at 686.9 eV and 685.5 eV. Both peaks correspond to F-Si bonds [47]. The peak at 685.5 eV could also be associated to the N 1s small peak detected at 402 eV, and would be related to salt formation $(NH_4)_2SiF_6$ as reported in reference [20]. This peak is slightly observable in Fig. 6 (b) that represents N1s spectra, and is evidenced with a dotted line.

In Fig. 5 (c), displaying the narrow scan of O 1s at -65°C for the two materials, a peak at 533.1 eV is detected on both materials and corresponds to O-SiF [37,46]. Two other peaks are also observed at 541.3 eV and 545.2 eV for Si_3N_4. They are related to physisorbed species that desorb once the sample is warmed up to 20°C. They are discussed further below.

Fig. 5 (d) presents the Si 2p spectra again at -65°C for the two materials. For a-Si, two structures are observed. The first one at 99.2 eV (2p3/2) corresponds to the a-Si bulk material, the second one located around 104 eV contains the contribution of SiOF species and initial SiO_2 surface oxide. To separate these two and evaluate the contribution of SiOF species, the experimental spectrum is fitted with two contributions. The first, labelled "a-Si substrate" in Fig. 5 (d), is taken from the reference experimental spectrum and therefore represents the contribution of the a-Si substrate, *i.e.* bulk a-Si and initial surface oxide; this envelope is fixed in terms of position, shape and width, the only free parameter being its height. The second contribution combines two "classical" Gaussian-Lorentzian shapes, one for each Si 2p spin-orbit component, using the usual Si 2p spin-orbit constraints (0.61 eV splitting, 0.5 (1/2)/(3/2) intensity ratio, identical full width at half maximum). This second contribution falls at 104.5 eV (2p3/2) which can correspond to Si-O(F) [46]. In comparison, the peak related to the native oxide is located at 103.5 eV [20,37,47]. Therefore we interpret the 104.5 eV peak as a clear indication of the presence

of SiOF species either due to physisorption of plasma species or to the fluorination of the native oxide layer. The slight mismatch between the reference component and the experimental data at the location of the initial oxide (103.5 eV) is a second indication of the fluorination of the oxide during the exposure to the plasma; subsequently the intensity of the SiOF component is probably slightly under estimated. However, this has no effect on the interpretation of the results as our purpose is to qualify the surface chemistry in order to progress in the understanding of the cryogenic nanoscale etching process and not to make a precise quantification (if ever possible) of the layer composition. For Si_3N_4, a large peak is observed; it is fitted using the same strategy: a first contribution (labelled "Si-N" in Fig. 5 (d) located at 102.2 eV (2p3/2) corresponding to the initial Si_3N_4 material, taken from the Si_3N_4 reference experimental spectrum and thus including the bulk Si_3N_4 and its surface oxide, and a second contribution at 104.5 eV (2p3/2) corresponding, as for a-Si, to fluorinated (Si-O(F) species) [46].

In summary, XPS spectra of Fig. 5 show that at -65°C, only a chemisorbed layer related to the native oxide fluorination is observed on a-Si, whereas for Si_3N_4, in addition to this chemisorption, mainly fluorine-based physisorbed species are observed.

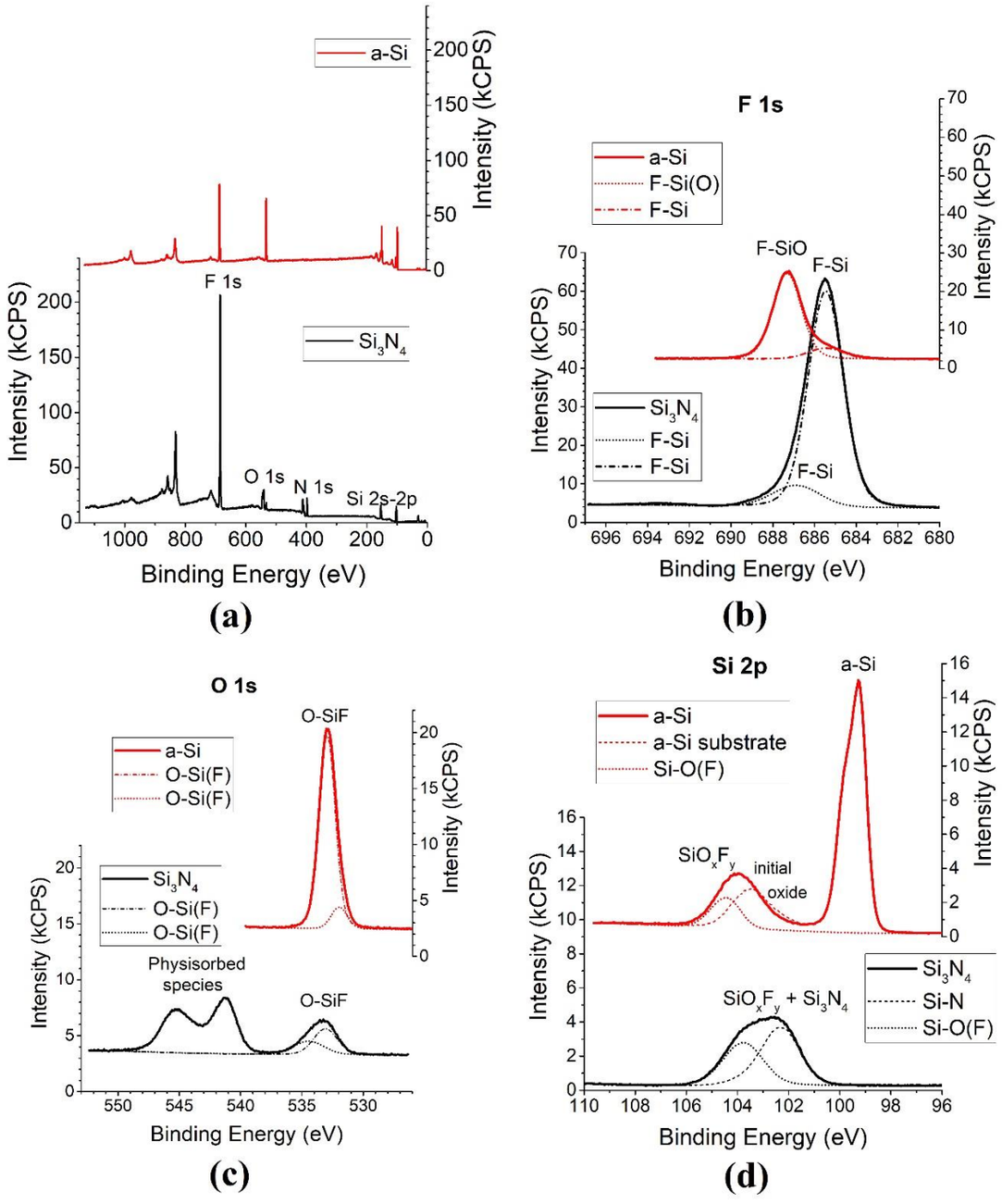

Fig. 5. XPS spectra on a-Si and Si_3N_4 coupon after SiF_4 / O_2 plasma exposure at -65°C (a) survey scan (b) F 1s, (c) O 1s, (d) Si 2p. For the latter (d) the "a-Si substrate" and "Si-N" components (dotted lines) are taken from the respective reference spectra.

(Experimental conditions: SiF_4 / O_2 plasma: 25%, 30 s, 3 Pa, 200 W)

In Fig. 6, narrow scans of the O 1s and N 1s core levels are presented, where unidentified peaks are detected on both materials. Peaks at 541.3 eV and 545.2 eV that are detected for the O 1s scan at -65°C on Si_3N_4 as discussed above are detected again at -100°C, but on both materials this time (Fig. 6 (a)). In Fig. 6 (b), in addition to the substrate peak N-Si at 397.9 eV for Si_3N_4 [32], two additional N peaks at 409 eV and 412.3 eV can be observed in the exact same conditions. They are only detected at -65°C on Si_3N_4 and at -100°C on both materials. Those peaks are observed at the same binding energies as long as fluorinated species are physisorbed. They only appear if a fluorine-based plasma is performed at low temperature. After warming the sample up to 20°C, they are no longer detected. To our knowledge, these peaks, which only appear at very low temperature, have never been reported. Fig. 6 suggests that these peaks originate from nitrogen-based species. They are probably due to N_2 molecules present in the chamber due to the residual leakage. They are dissociated into N radicals in the plasma and react at the surface to form nitrogen based physisorbed species.

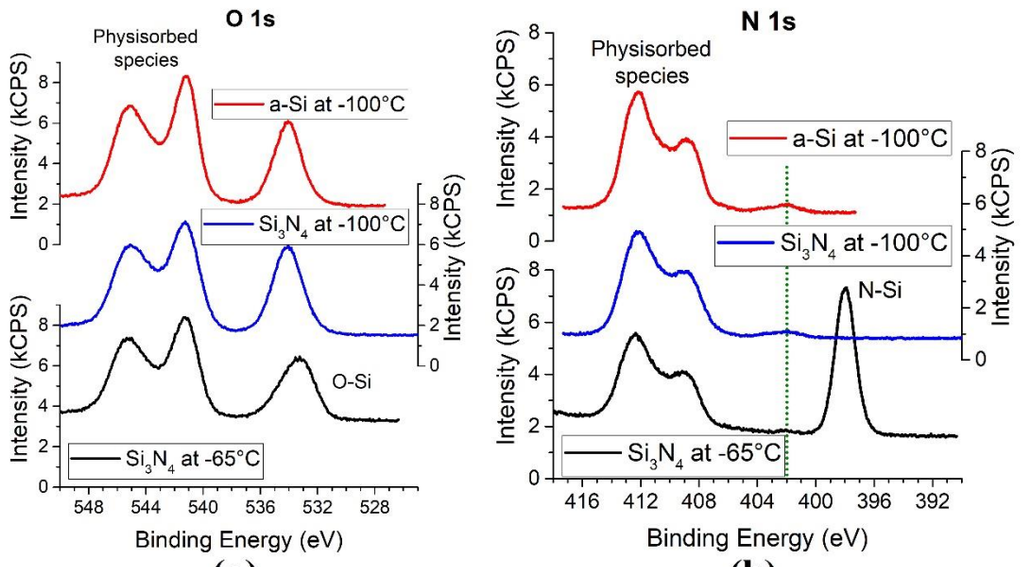

Fig. 6. (a) O 1s and (b) N 1s spectra on a-Si and Si_3N_4 coupon after SiF_4 / O_2 plasma exposure at -65°C and -100°C (Experimental conditions: SiF_4 / O_2 plasma: 25%, 30 s, 3 Pa, 200 W)

III.2 SiO_xF_y modification layer for nanoscale etching

The XPS results have shown that the SiF_4 / O_2 plasma fluorinates both the a-Si and Si_3N_4 surfaces, and that decreasing the temperature enhances the physisorption of fluorinated species at the surface. This fluorinated layer can be used as a reservoir of reactive species. When the layer is exposed to an argon plasma, it can therefore activate the etching of a-Si and Si_3N_4 material. A process consisting of alternating SiF_4 / O_2 plasma deposition step and Ar activation etch step is proposed as in an Atomic Layer Etching (ALE) process. The SiF_4 / O_2 plasma is used for the surface modification step and the Ar plasma step is used to remove the modified layer. The time chart of the process is presented in Fig. 7.

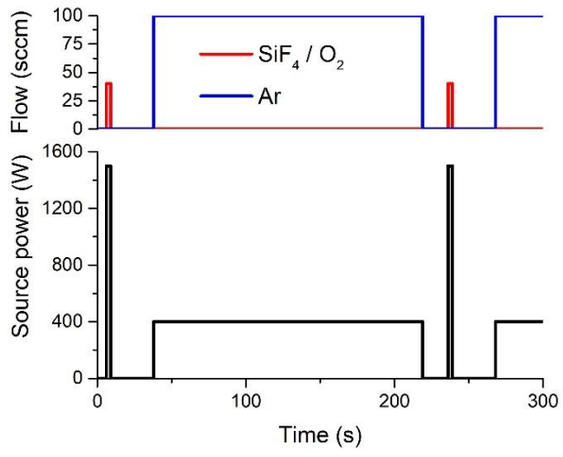

Fig. 7. Time chart of the alternating process

First, a SiF_4 / O_2 plasma was performed for 3 s. SiF_4 and O_2 flows were 5 and 35 sccm respectively (12.5% of SiF_4 in the mixture). The pressure was 0.7 Pa and the plasma source power was 1500 W and no bias was applied to the substrate. Then, a pumping step as long as 30 s was used to evacuate all the species of the plasma that did not deposit on the surface.

Afterwards, an Ar plasma was ignited for 3 min to etch the modified layer. The Ar flow was 100 sccm, the pressure was set to 3.1 Pa, the plasma source power was 400 W and no bias was applied. Finally, a second pumping step was performed to ensure the removal of all the etch by-products before starting a new cycle.

These steps were repeated in order to perform 8 cycles at 5 different substrate temperatures, from +20°C to -100°C.

The thickness evolution was monitored by *in situ* SE in kinetic mode on a-Si and by *ex situ* SE on both a-Si and Si_3N_4 (Fig. 8).

Figure 8. (a) shows the thickness evolution versus time. At 20°C, the a-Si thickness increases during SiF_4 / O_2 plasma by about 0.2 nm per cycle and the subsequent Ar plasma does not significantly etch the deposited layer. After the 8 cycles, the layer thickness increases up to 1.6 nm on a-Si: the process is in deposition regime. When the temperature is decreased to -40°C, the deposited amount remains close to 0.2 nm during each SiF_4 / O_2 plasma step. But, the deposited layer is almost completely etched during the Ar plasma. Hence, only a thickness increase of 0.5 nm is obtained after the 8 cycles.

At -65°C, the process evolves to an etching regime. About 3 cycles are necessary to reach the steady state of the etch regime. Indeed, after the first two cycles, the thickness first increased, and then started to decrease after the third cycle. In Fig. 8 (b), a zoom on the 4th cycle is shown. The deposited amount of SiO_xF_y layer is slightly lower than for processes at higher temperature (0.17 nm per cycle). During the Ar plasma, the deposited layer is removed as well as part of the substrate thickness. At the end of the process, 0.4 nm of a-Si is etched.

When the temperature is decreased to -80°C and lower, the process is clearly in etching regime from the first cycle. The zoom on the fourth cycle at -100°C presented in Fig. 8 (c) shows that the a-Si is etched even during the SiF_4 / O_2 plasma. Hence, after 8 cycles, it was possible to etch about 6.5 nm of a-Si.

Fig. 8 (d) shows the total thickness variation as a function of temperature for both a-Si and Si_3N_4 samples. As expected from the XPS results, i.e. with a comparable deposited SiO_xF_y film, a similar behavior is observed for the two materials for temperatures higher than -40°C and at -100°C. Indeed, at -40°C, almost the same SiO_xF_y thickness increase is measured for both materials. At -100°C, both materials are etched at nearly the same etch rate. However, for temperatures close to -65°C, Si_3N_4 is etched much faster than a-Si with a selectivity of Si_3N_4 over a-Si as high as 13.5.

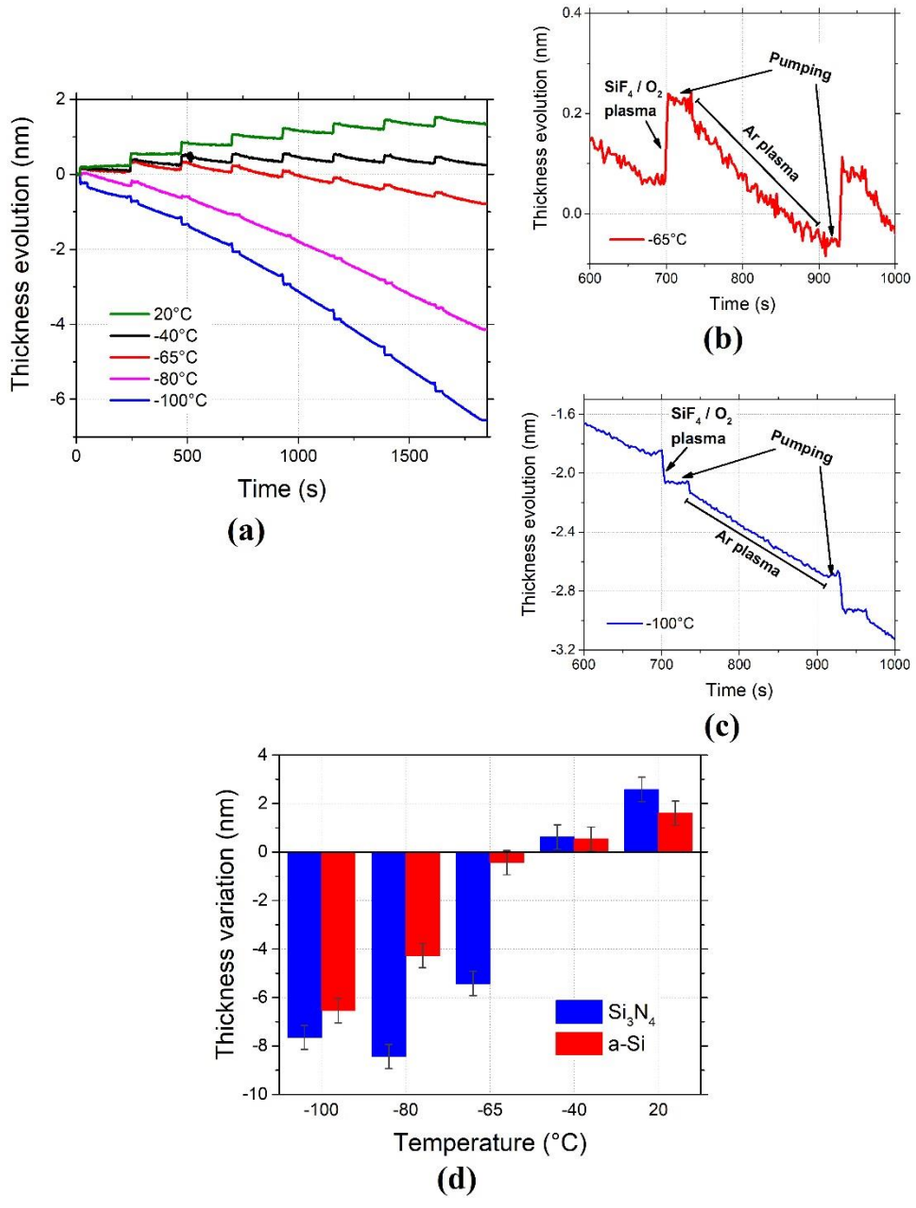

Fig. 8. Effect of the temperature in a process alternating SiF_4 / O_2 and Ar plasma (a) Thickness evolution measured by SE in kinetic mode during 8 cycles on a-Si, (b) zoom on cycle #4 at -65°C, (c) zoom on cycle #4 at -100°C, (d) thickness variation measured by ex-situ SE on a-Si and Si_3N_4

(Experimental conditions: SiF_4 / O_2 plasma: 25%, 3 s, 0.7 Pa, 1500 W, Pumping: 30 s, 0.1 Pa, Ar plasma: 3min, 3.1 Pa, 400 W, Pumping: 15 s, 0.1 Pa)

IV. Discussions

According to the obtained results, a sketch illustrating the surface reactions and state is presented in Fig. 9 to summarize the involved mechanisms. At -40°C, during the SiF_4 / O_2 plasma, there is a competition between oxygen and fluorine species to adsorb at the surface. As a result, the oxide on top of each material is fluorinated and a dense SiO_xF_y layer is chemisorbed on the surface (Fig. 9 (a)). This layer is stable even at room temperature and is not very rich in fluorine. Consequently, the layer will be hardly etched by low Ar ion energy bombardment as reported in [35]. Thus, the SiO_xF_y deposited layer will prevent from etching. The same layer is formed on a-Si surface when the deposition is performed at -65°C (Fig. 9 (a)). However, on Si_3N_4, the nitrogen from the layer may be consumed either by oxygen or hydrogen atoms from residual water molecules present in the chamber. In the first case, NO_x will form at the surface and will desorb; in the second case, NH_3 will form and will desorb from the surface. In both cases, Si active sites are created, improving the possibility to adsorb SiF_x species. Note that nitrogen could also react with fluorine to form NF_3 molecules, which are volatile. However, the fluorine concentration is quite high at the surface. SiF_x species coming from the plasma are deposited on the surface increasing the concentration of fluorine in the layer. Thus, the physisorption of fluorinated species is enhanced from -65°C for Si_3N_4 (Fig. 9 (b)). Consequently, the layer is richer in fluorine species, which will enable the removal of Si during

the Ar plasma. Moreover, as the layer is composed of both chemisorbed and physisorbed species, the layer is less dense and easier to etch (Fig. 9 (b)).

At -100°C, the physisorption of fluorinated species is significantly enhanced for both a-Si and Si_3N_4 (Fig. 9 (b)). Consequently, in addition to the chemisorbed species, a significant part of physisorbed species will participate to the etching of both layers (Fig. 9 (c)). Thus, the selectivity at this temperature becomes lower than at -65°C.

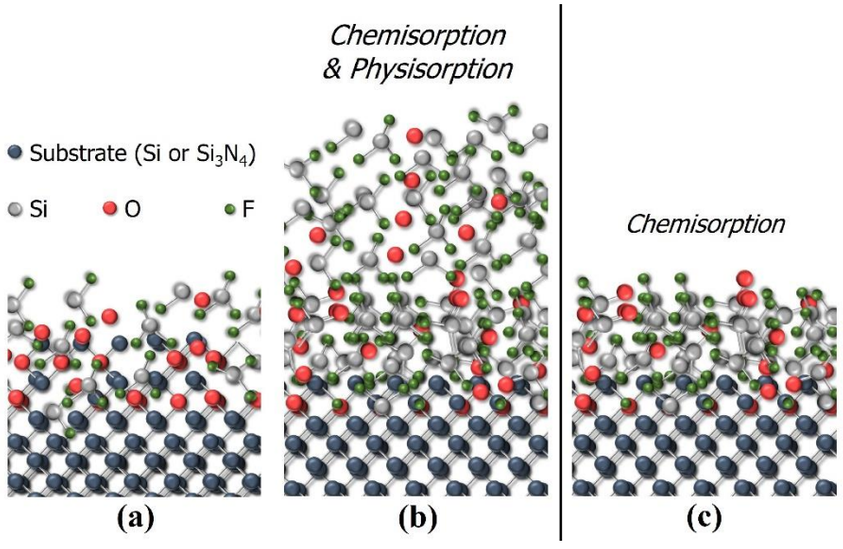

Fig. 9. Surface state after deposition (a) at T > -65°C for Si_3N_4 and T > -100°C for a-Si (b) at T ≤ -65°C for Si_3N_4 and T≤ -100°C for a-Si and (c) after etching for both materials

Conclusion

Quasi *in situ* XPS measurements have been carried out on a-Si and Si_3N_4 materials after a SiF_4 / O_2 plasma process at different temperatures. At -40°C, the composition of the grown SiO_xF_y layer is similar for both materials. At -65°C, the fluorine content of the SiO_xF_y layer significantly increases on Si_3N_4 whereas it remains at about the same level on a-Si. At -100°C, the fluorine content is high on both materials with about the same percentage. When the sample is warmed back to room temperature, the fluorine content on both materials significantly

decreases indicating that a significant part of the SiO_xF_y layer is composed F-based physisorbed species.

By taking advantage of this temperature dependency for F-rich species physisorption, it was possible to develop a nanoscale etching process with a selectivity as high as 13.5 between Si_3N_4 and a-Si. It consists of an alternation of SiO_xF_y deposition step in SiF_4 / O_2 plasma and Ar removing step on the model of ALE processes. A temperature threshold between deposition and etching regimes has been evidenced: by decreasing the temperature, etching can dominate deposition in average per cycle. Close to -65°C, the deposited SiO_xF_y layer acts as an etch stop layer on a-Si while it contributes to etch Si_3N_4. On Si_3N_4, a part of the oxygen is consumed by reacting with N atoms leading to a lower concentration of oxygen in the SiO_xF_y. Thus, selective etching is achieved at this very temperature on SiO_xF_y during the argon plasma, which releases more fluorine that will etch the Si_3N_4. Close to -100°C, a F-rich SiO_xF_y layer is grown on both materials, causing etching on Si_3N_4 and a-Si at almost the same rate, with a loss of selectivity between the two materials.

In conclusion, it is possible to tune the concentration of reactive species, more specifically fluorine, in the SiO_xF_y layer by modifying the sample temperature. The threshold temperature between deposition and etching per cycle is different between a-Si and Si_3N_4, which enables to achieve a high etching selectivity of Si_3N_4 over Si at nanoscale.

ACKNOWLEDGEMENT

The authors gratefully thank Shigeru Tahara from TEL for all the helpful discussions and also Kumiko Yamazaki and Nagisa Sato from TEL for their support to the project.

This work was supported by CERTeM 5.0 platform, which provides most of the equipment. It is also partially supported by ANR, under the project name PSICRYO (ANR-20-CE24-0014).

The CNRS-Réseau des Plasmas Froids is also acknowledged for giving access to the Optimist platform.

AUTHOR DECLARATIONS

CONFLICT OF INTEREST

The authors have no conflicts of interest to declare.

DATA AVAILABILITY

The data that support the findings of this study are available from the corresponding author upon reasonable request.

References

[1] G. Antoun, P. Lefaucheux, T. Tillocher, R. Dussart, K. Yamazaki, K. Yatsuda, J. Faguet, and K. Maekawa, Appl. Phys. Lett. **115**, 153109 (2019).

[2] A.B. Kletskii and L.E. Petric, Zh. Fiz. Khim. **41**, 1183 (1967).

[3] V. Renaud, C. Petit-Etienne, J.-P. Barnes, J. Bisserier, O. Joubert, and E. Pargon, Journal of Applied Physics **126**, 243301 (2019).

[4] S. Sridhar, P.L.G. Ventzek, and A. Ranjan, J. Vac. Sci. Technol. A **38**, 043007 (2020).

[5] Y. Wang and L. Luo, J. Vac. Sci. Technol. A **16**, 1582 (1998).

[6] B.E.E. Kastenmeier, P.J. Matsuo, and G.S. Oehrlein, J. Vac. Sci. Technol. A **17**, 3179 (1999).

[7] M. Schaepkens, T.E.F.M. Standaert, N.R. Rueger, P.G.M. Sebel, G.S. Oehrlein, and J.M. Cook, J. Vac. Sci. Technol. A **17**, 26 (1999).

[8] N. Gellrich and R. Kirchmann, US6569773B1 (2003).

[9] T.E.F.M. Standaert, C. Hedlund, E.A. Joseph, G.S. Oehrlein, and T.J. Dalton, J. Vac. Sci. Technol. A **22**, 53 (2004).

[10] S. Lee, J. Oh, K. Lee, and H. Sohn, J. Vac. Sci. Technol. B **28**, 8 (2010).

[11] D. Nakayama, A. Wada, T. Kubota, R. Bruce, R.M. Martin, M. Haass, N. Fuller, and S. Samukawa, J. Phys. D: Appl. Phys. **46**, 205203 (2013).

[12] Y. Kondo, K. Ishikawa, T. Hayashi, Y. Miyawaki, K. Takeda, H. Kondo, M. Sekine, and M. Hori, Jpn. J. Appl. Phys. **54**, 040303 (2015).

[13] M. Bouchilaoun, A. Soltani, A. Chakroun, A. Jaouad, M. Darnon, F. Boone, and H. Maher, Phys. Status Solidi A **215**, 1700658 (2018).

[14] N. Lim, A. Efremov, and K.-H. Kwon, Thin Solid Films **685**, 97 (2019).

[15] S.-N. Hsiao, K. Ishikawa, T. Hayashi, J. Ni, T. Tsutsumi, M. Sekine, and M. Hori, Appl. Surf. Sci. **541**, 148439 (2021).

[16] T. Matsuura, Y. Honda, and J. Murota, Appl. Phys. Lett. **74**, 3573 (1999).

[17] N. Posseme, O. Pollet, and S. Barnola, Appl. Phys. Lett. **105**, 051605 (2014).

[18] C. Li, D. Metzler, C.S. Lai, E.A. Hudson, and G.S. Oehrlein, J. Vac. Sci. Technol. A **34**, 041307 (2016).

[19] S.D. Sherpa and A. Ranjan, J. Vac. Sci. Technol. A **35**, 01A102 (2017).

[20] N. Posseme, V. Ah-Leung, O. Pollet, C. Arvet, and M. Garcia-Barros, J. Vac. Sci. Technol. A **34**, 061301 (2016).

[21] S.D. Sherpa, P.L.G. Ventzek, and A. Ranjan, J. Vac. Sci. Technol. A **35**, 05C310 (2017).

[22] W.-H. Kim, D. Sung, S. Oh, J. Woo, S. Lim, H. Lee, and S.F. Bent, J. Vac. Sci. Technol. A **36**, 01B104 (2017).

[23] S.G. Walton, D.R. Boris, S.C. Hernández, E.H. Lock, Tz.B. Petrova, G.M. Petrov, A.V. Jagtiani, S.U. Engelmann, H. Miyazoe, and E.A. Joseph, Microelectron. Eng. **168**, 89 (2017).

[24] C.M. Huard, S. Sriraman, A. Paterson, and M.J. Kushner, J. Vac. Sci. Technol. A **36**, 06B101 (2018).

[25] K.-Y. Lin, C. Li, S. Engelmann, R.L. Bruce, E.A. Joseph, D. Metzler, and G.S. Oehrlein, J. Vac. Sci. Technol. A **36**, 040601 (2018).

[26] K. Nakane, R.H.J. Vervuurt, T. Tsutsumi, N. Kobayashi, and M. Hori, ACS Appl. Mater. Interfaces **11**, 37263 (2019).

[27] K. Shinoda, N. Miyoshi, H. Kobayashi, M. Izawa, T. Saeki, K. Ishikawa, and M. Hori, J. Vac. Sci. Technol. A **37**, 051002 (2019).

[28] Y. Kim, S. Lee, Y. Cho, S. Kim, and H. Chae, J. Vac. Sci. Technol. A **38**, 022606 (2020).

[29] R.J. Gasvoda, Z. Zhang, S. Wang, E.A. Hudson, and S. Agarwal, J. Vac. Sci. Technol. A **38**, 050803 (2020).

[30] E. Cheng and G.S. Hwang, Applied Surface Science **543**, 148557 (2021).

[31] N. Miyoshi, K. Shinoda, H. Kobayashi, M. Kurihara, Y. Kouzuma, and M. Izawa, J. Vac. Sci. Technol. A **39**, 052601 (2021).

[32] S.-N. Hsiao, K. Nakane, T. Tsutsumi, K. Ishikawa, M. Sekine, and M. Hori, Appl. Surf. Sci. **542**, 148550 (2021).

[33] Y. Kataoka, S. Saito, and K. Omiya, J. Electrochem. Soc. **146**, 3435 (1999).

[34] G. Antoun, R. Dussart, T. Tillocher, P. Lefaucheux, C. Cardinaud, A. Girard, S. Tahara, K. Yamazaki, K. Yatsuda, J. Faguet, and K. Maekawa, Jpn. J. Appl. Phys. **58**, SEEB03 (2019).

[35] G.S. Oehrlein and Y. Kurogi, Mater. Sci. Eng., R **24**, 153 (1998).

[36] S. Aachboun, P. Ranson, C. Hilbert, and M. Boufnichel, J. Vac. Sci. Technol. A **18**, 1848 (2000).

[37] R. Dussart, M. Boufnichel, G. Marcos, P. Lefaucheux, A. Basillais, R. Benoit, T. Tillocher, X. Mellhaoui, H. Estrade-Szwarckopf, and P. Ranson, J. Micromech. Microeng. **14**, 190 (2003).

[38] R. Dussart, X. Mellhaoui, T. Tillocher, P. Lefaucheux, M. Boufnichel, and P. Ranson, Microelectron. Eng. **84**, 1128 (2007).

[39] J. Pereira, L.E. Pichon, R. Dussart, C. Cardinaud, C.Y. Duluard, E.H. Oubensaid, P. Lefaucheux, M. Boufnichel, and P. Ranson, Appl. Phys. Lett. **94**, 071501 (2009).

[40] M. Gaudig, J. Hirsch, V. Naumann, M. Werner, S. Großer, C. Hagendorf, N. Bernhard, and D. Lausch, J. Appl. Phys **121**, 063301 (2017).

[41] S. Tachi, K. Tsujimoto, and S. Okudaira, Appl. Phys. Lett. **52**, 616 (1988).

[42] G. Antoun, A. Girard, T. Tillocher, P. Lefaucheux, J. Faguet, K. Maekawa, C. Cardinaud, and R. Dussart, ECS J. Solid State Sci. Technol. **11**, 013013 (2022).

[43] G. Antoun, T. Tillocher, P. Lefaucheux, J. Faguet, K. Maekawa, and R. Dussart, Sci Rep **11**, 357 (2021).

[44]Copyright © 2005 Casa Software Ltd.

[45] Ch. Cardinaud and G. Turban, Applied Surface Science **45**, 109 (1990).

[46] G.S. Oehrlein, K.K. Chan, M.A. Jaso, and G.W. Rubloff, J. Vac. Sci. Technol. A **7**, 1030 (1989).

[47] C. Cardinaud, A. Rhounna, G. Turban, and B. Grolleau, J. Electrochem. Soc. **135**, 1472 (1988).

Figure captions

Fig. 1. Ellipsometric parameters Is and Ic measured and fitted as a function of the photon energy for a SiO_xF_y layer deposited at -40°C on (a) a-Si, (b) Si_3N_4 (Experimental conditions: SiF_4 / O_2: 25%, Source: 1500 W, 1.2 Pa, 30 s)

Fig. 2. Sketch of the OPTIMIST Platform

Fig. 3. Thickness variation of a-Si and Si_3N_4 at different temperatures, after SiF_4 / O_2 plasma (Experimental conditions: SiF_4 / O_2: 25%, Source: 1500 W, 1.2 Pa, 30 s)

Fig. 4. XPS average quantification of the surface composition after SiF_4 / O_2 plasma and after warming the sample back to 20°C, (a) on a-Si and (b) on Si_3N_4 (Experimental conditions: SiF_4 / O_2 plasma: 25%, 30 s, 3 Pa, 200 W)

Fig. 5. XPS spectra on a-Si and Si_3N_4 coupon after SiF_4 / O_2 plasma exposure at -65°C (a) survey scan (b) F 1s, (c) O 1s, (d) Si 2p. For the latter (d) the "a-Si substrate" and "Si-N" components (dotted lines) are taken from the respective reference spectra. (Experimental conditions: SiF_4 / O_2 plasma: 25%, 30 s, 3 Pa, 200 W)

Fig. 6. (a) O 1s and (b) N 1s spectra on a-Si and Si_3N_4 coupon after SiF_4 / O_2 plasma exposure at -65°C and -100°C (Experimental conditions: SiF_4 / O_2 plasma: 25%, 30 s, 3 Pa, 200 W)

Fig. 7. Time chart of the alternating process

Fig. 8. Effect of the temperature in a process alternating SiF_4 / O_2 and Ar plasma (a) Thickness evolution measured by SE in kinetic mode during 8 cycles on a-Si (b) zoom on cycle #4 at -65°C, (c) zoom on cycle #4 at -100°C, (d) thickness variation measured by ex-situ SE on a-Si and Si_3N_4

Fig. 9. Surface state after deposition (a) at T > -65°C for Si_3N_4 and T > -100°C for a-Si (b) at T ≤ -65°C for Si_3N_4 and T≤ -100°C for a-Si and (c) after etching for both materials

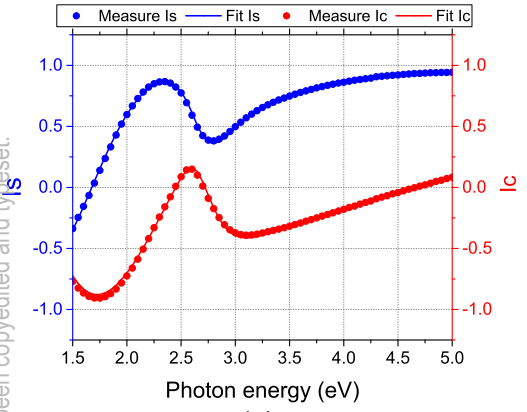

(a)

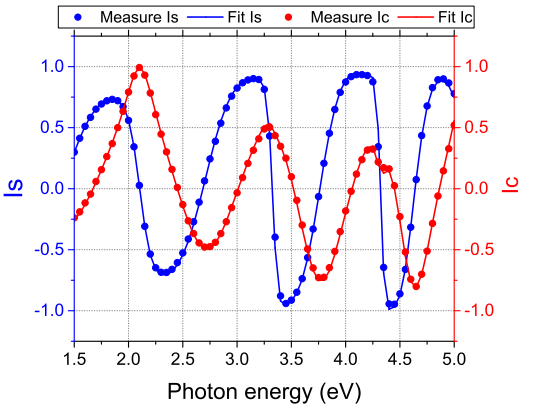

(b)

Journal of Vacuum Science Technology A

ACCEPTED MANUSCRIPT

PLEASE CITE THIS ARTICLE AS DOI: 10.1116/6.0001885

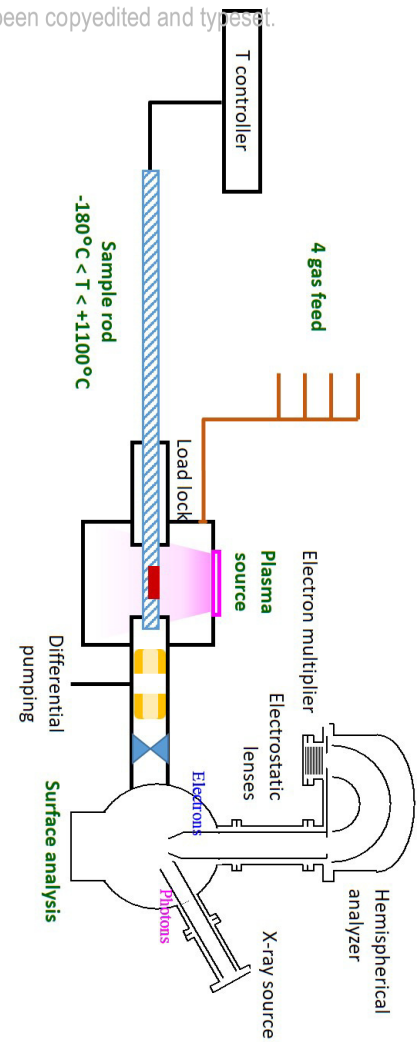

Journal of Vacuum Science Technology A

ACCEPTED MANUSCRIPT

This is the author's peer reviewed, accepted manuscript. However, the online version of record will be different from this version once it has been copyedited and typeset.
PLEASE CITE THIS ARTICLE AS DOI: 10.1116/6.0001885

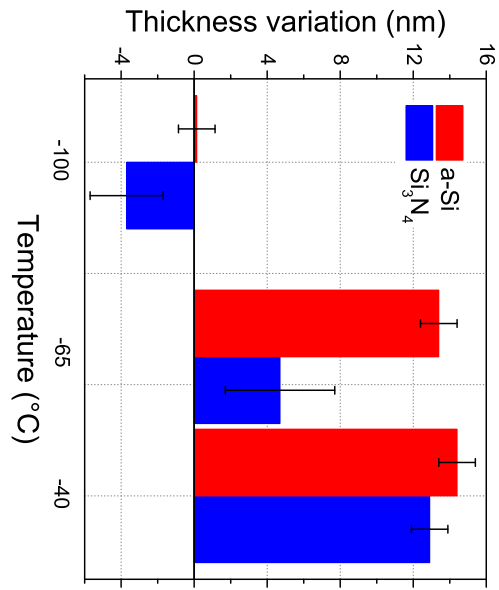

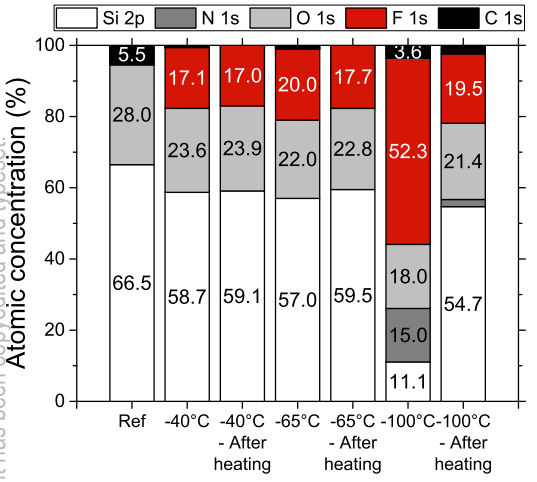

(a)

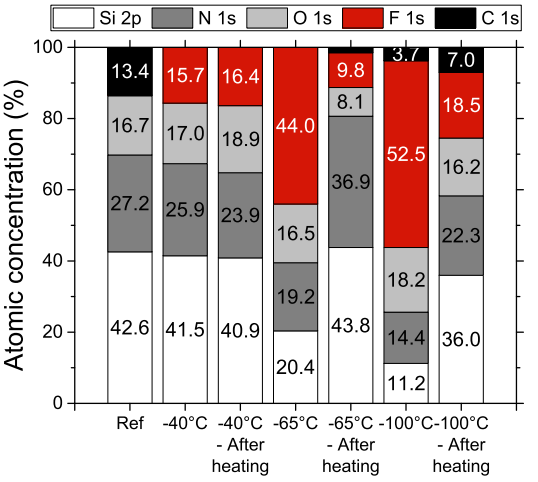

(b)

Journal of Vacuum Science Technology A

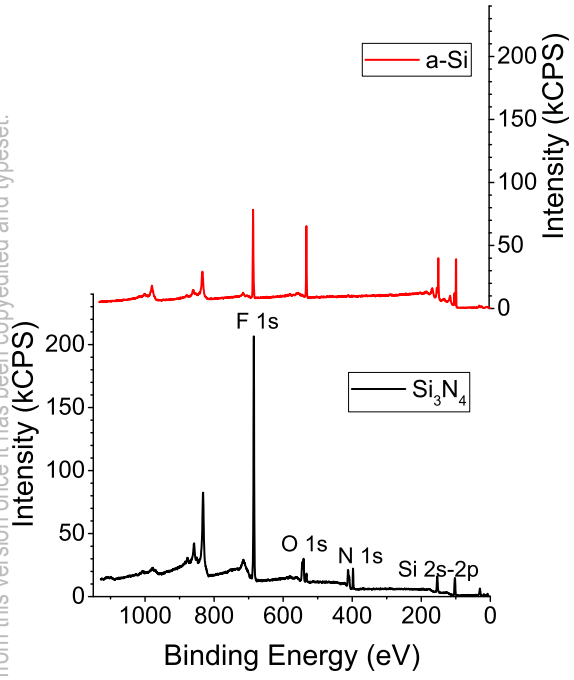

(a)

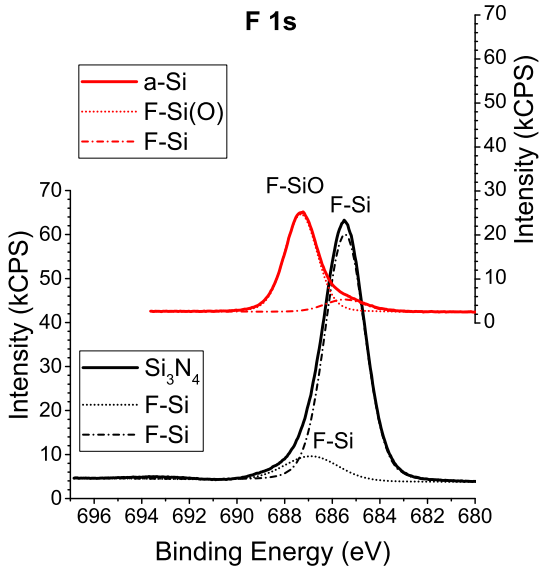

(b)

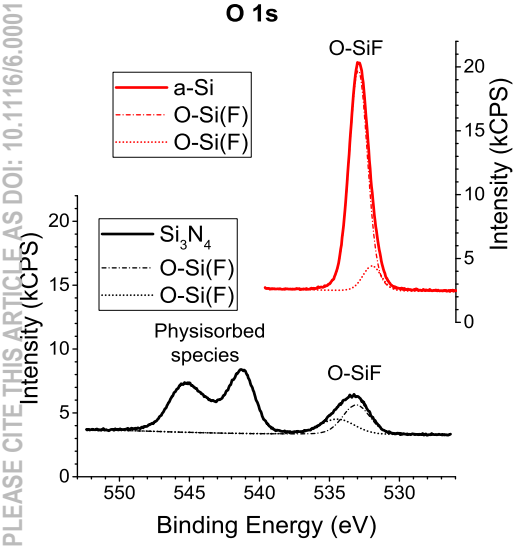

(c)

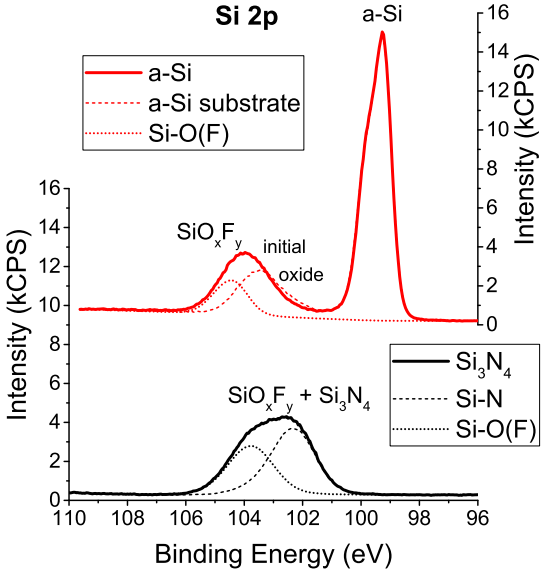

(d)

Journal of Vacuum Science Technology A

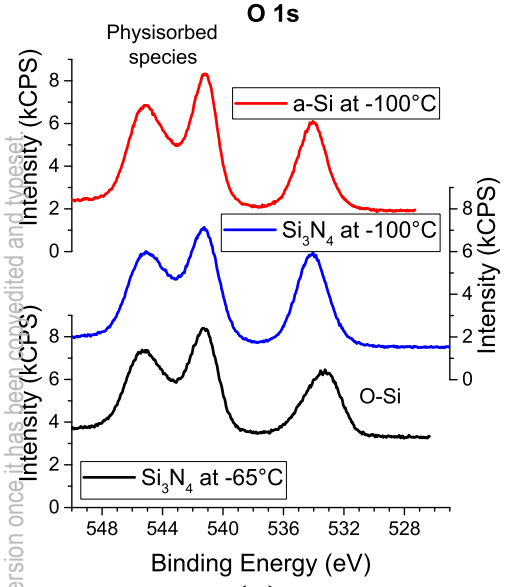

(a)

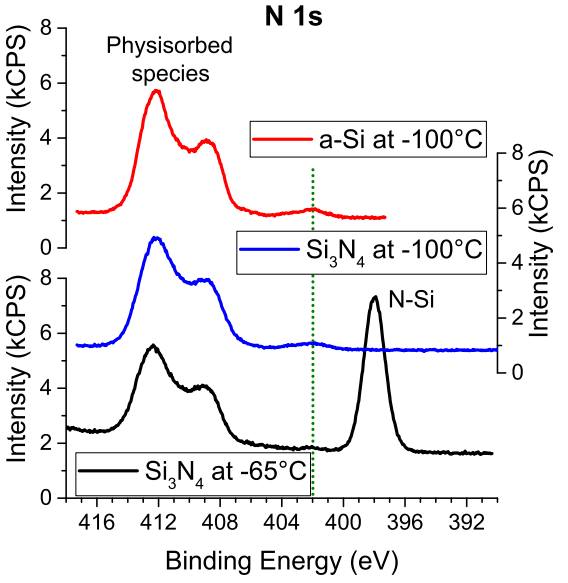

(b)

Journal of Vacuum Science Technology A

ACCEPTED MANUSCRIPT

This is the author's peer reviewed, accepted manuscript. However, the online version of record will be different from this version once it has been copyedited and typeset.
PLEASE CITE THIS ARTICLE AS DOI: 10.1116/6.0001885

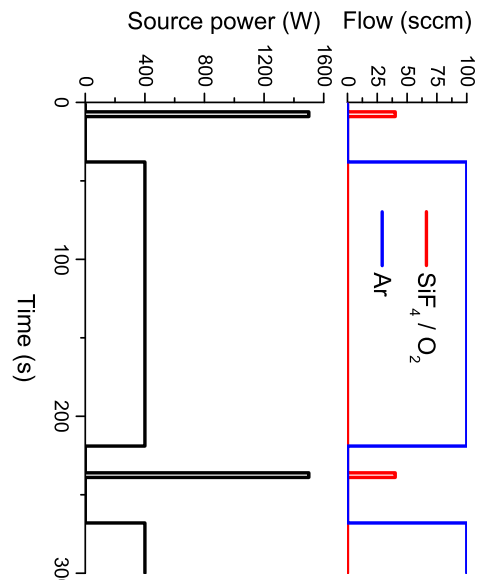

Journal of Vacuum Science Technology A

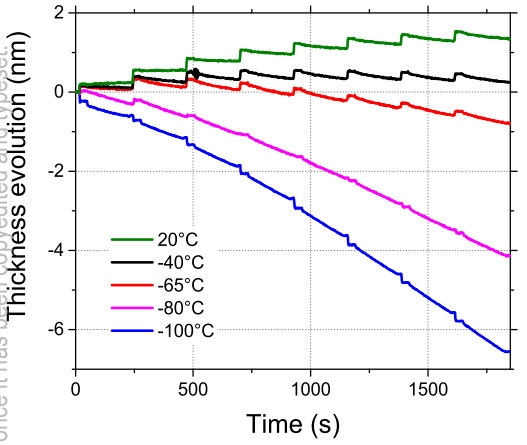

(a)

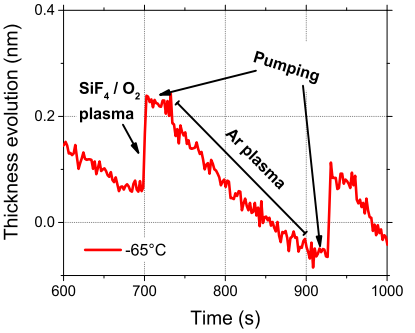

(b)

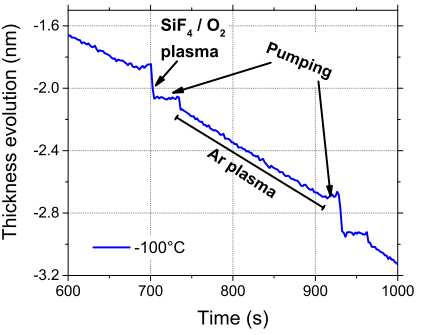

(c)

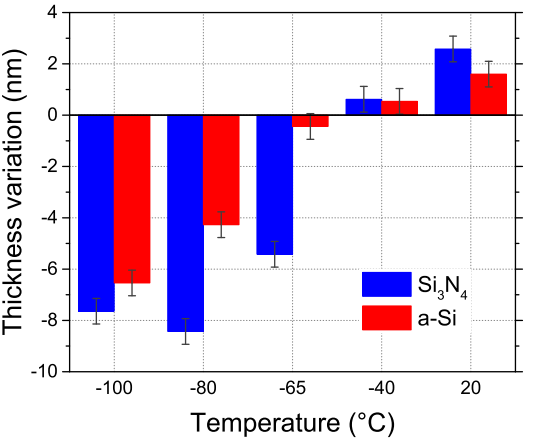

(d)

Journal of Vacuum Science Technology A

ACCEPTED MANUSCRIPT

PLEASE CITE THIS ARTICLE AS DOI: 10.1116/6.0001885